Multivalent Counterions Diminish the Lubricity of Polyelectrolyte Brushes

J. Yu[1,2,3†], N.E. Jackson[1,2†], X. Xu[4], Y. Morgenstern[5], Y. Kaufman[5], M. Ruths[4], J.J. de Pablo[1,2*], M. Tirrell[1,2*]

Affiliations

[1]Institute for Molecular Engineering, University of Chicago, Chicago, IL 60637, USA.

[2]Institute for Molecular Engineering, Argonne National Laboratory, Lemont, IL 60439, USA.

[3]School of Materials Science and Engineering, Nanyang Technological University, Singapore 639798.

[4]Department of Chemistry, University of Massachusetts Lowell, Lowell, MA 01854, USA.

[5]Zuckerberg Institute for Water Research, The Jacob Blaustein Institutes for Desert Research, Ben-Gurion University of the Negev, Midreshet Ben-Gurion, Israel

* Correspondence to: depablo@uchicago.edu, mtirrell@uchicago.edu

† = These authors contributed equally to this work.

Abstract

Polyelectrolyte brushes provide wear protection and lubrication in many technical, medical, physiological and biological applications. Wear resistance and low friction are attributed to counterion osmotic pressure and the hydration layer surrounding the charged polymer segments. However, the presence of multivalent counterions in solution can strongly affect the interchain interactions and structural properties of brush layers. We evaluated the lubrication properties of polystyrene sulfonate brush layers sliding against each other in aqueous solutions containing increasing concentrations of counterions. The presence of multivalent ions (Y^{3+}, Ca^{2+}, Ba^{2+}), even at minute concentrations, dramatically increases the friction forces between brush layers due to electrostatic bridging and brush collapse. Our results suggest the lubricating properties of polyelectrolyte brushes in multivalent solution are hindered relative to those in monovalent solution.

Soft interfaces consisting of charged macromolecules are the norm in biology, including the cellular glycocalyx (*1*), the surface of articular cartilage (*2, 3*), and the interfaces between mineralized collagen in bone (*4*). Commercial products, such as those for personal care, medical prostheses (e.g., joint replacement), anti-fogging surfaces, and DNA brushes for synthetic biology and gene chips (*5, 6*), also often rely on highly hydrated polyelectrolyte brush interfaces (*7-11*). Characterization of the tribological and dynamical properties of polyelectrolyte brushes has been of interest because of their tunable wetting properties (*12*), strong osmotic repulsion (*13*), compression-induced interpenetration (*14*), durability (*15*), and solvent response (*16*). Polyelectrolyte brush structure can be influenced by environmental modulations, (e.g. pH, temperature and added salt) (*17-19*). Sharp changes in brush height and morphology were observed as a function of the concentration of added multivalent ions in experiments (*20, 21*), MD simulation (*22, 23, 24*), and theory (*25*). Surface forces apparatus (SFA) experiments have detected attractive interactions consistent with multivalent ion-induced bridging between polyelectrolyte brush layers on apposing surfaces (*26*). However, most tribological studies of polyelectrolyte brushes have been limited to pure water or monovalent salt solutions (*10, 13, 27*). Considering the prevalence of multivalent ions in biological systems and industrial formulations (*28, 29*), a concrete understanding of their role in polyelectrolyte brush lubrication is of importance.

Densely tethered polystyrene sulfonate (PSS) brushes were grown from mica surfaces using a surface initiated atom transfer radical polymerization method (*21*). The kinetic friction force (F_k) between apposing brush surfaces was measured as a function of their absolute separation distance (D), compression load (L) and sliding velocity ($V_{||}$) in a droplet of aqueous solution using a surface forces apparatus (model SFA 2000, SurForce LLC) (Fig. 1A). In 6 mM $NaNO_3$, the PSS brushes

showed excellent lubrication properties. The friction forces between two brush layers sliding against each other at a velocity of ~ 4.8 μm/s were just above the detection limit (~ 5 μN) of the friction sensor up to a load of 13 mN (Fig. 1B, insert, and Fig. S1). The coefficient of friction (COF), μ, between the two brush layers, defined as dF_k/dL, was smaller than 0.001. The pressure between apposing surfaces in this load regime was estimated to be ~ 5 MPa. Both μ and the pressure are within the range encountered in human knee joints (*30*). As the load was increased above 13 mN, the friction force was observed to increase linearly with a slope of μ = 0.005 ± 0.001, which is still a very low friction coefficient. Increasing the monovalent salt concentration to 0.15 M screened electrostatic repulsion between charged PSS segments, which facilitated inter-chain penetration of the apposing brushes, leading to an increased μ of 0.03 (Fig. S1B). Introducing trivalent Y^{3+} ions into the solution dramatically increased the friction forces. In a solution containing 3 mM $NaNO_3$ and 0.5 mM $Y(NO_3)_3$ (maintaining the total ionic strength at 6 mM), large friction forces were measured even at very small loads (Figs. 1B, S1, S2) with distinct features on the friction traces (raw data) measured (Fig. S3). μ was in the range 0.15–0.3, two orders of magnitude larger than in 6 mM $NaNO_3$.

To determine the tribological impact of multivalent ions, the normal and friction forces of apposing brushes were measured at constant contact point and ionic strength (6 mM) for four concentrations of Y^{3+} (0, 0.01, 0.1, and 0.5 mM) and four concentrations of Ca^{2+} and Ba^{2+} (0, 0.01, 0.1, 1.0 mM) (Fig. 1C,D,E, S4–S8). Sliding was studied at low loads to avoid surface damage. In 6 mM $NaNO_3$, a repulsive force was detected at a separation distance of 600 nm, and rapidly increased upon compression (Fig. 1C). Friction forces measured following the normal force measurement were extremely low (< 10 μN) (Fig. 1B) for the range of load (0–6 mN) investigated (Fig. 1D). The presence of Y^{3+}, even at low concentration (0.01 mM), decreased the range of repulsion from 600

nm to 480 nm (Fig. 1C). The brushes were still in the extended state, as Atomic force microscopy (AFM) measurements in solution showed relatively homogeneous height images for PSS brush layers in pure 6 mM $NaNO_3$ and in 0.01 mM Y^{3+} (Fig. 2A,B and Fig. S9). However, the addition of 0.01 mM Y^{3+} significantly affected the friction force (Fig. 1D), which was very small at loads up to 3 mN, and then rapidly increased. Despite showing distinct differences in the friction forces at loads above 3 mN, the PSS brushes had similar heights in pure 6 mM $NaNO_3$ and in 0.01 mM Y^{3+} (Fig. S2). We hypothesize that this increase was due to enhanced chain interpenetration of the apposing brushes at higher compression (*31*), leading to more bridging events between the negatively charged sulfonate groups, mediated by the multivalent ions. This will be addressed in the MD simulations described below.

In solutions containing higher concentrations (0.1 and 0.5 mM) of Y^{3+}, the range of separation distances over which repulsion was measured during compression rapidly decreased to less than 300 nm, and strong hysteresis was measured during the separation (Fig. 1C). In both conditions, the friction forces were larger than those measured at lower Y^{3+} concentration: a high friction force of ~ 0.1 mN was evident even at very low load (0.2 mN), and then rapidly increased with the load (Fig. 1D). Similar trends, with quantitative differences depending on the ion, in normal and friction forces were observed for divalent ions (Ca^{2+} and Ba^{2+}), with small friction forces at low concentrations (0.01 mM) and dramatically increasing forces at higher concentrations (0.1 mM and 1 mM) (Fig. 1E, S4–S8). Polyelectrolyte brushes can form pinned-micelle like inhomogeneous structures in the presence of multivalent counterions due to electrostatic bridging.(*22*, *23*, *24*) AFM measurements confirmed that in 0.1 and 0.5 mM Y^{3+}, and 1 mM Ba^{2+} solution, the brush layer collapsed into pinned-micelle like structures (Figs. 2C,D, S10–S12) accompanied by a stark

decrease in brush height (Figs. 2E, S2, S8). Although the PSS brush also collapsed in 1 mM Ca^{2+} solution (Fig. S7), no clear micelle like structure was observed by AFM (Fig. S10). Additionally, AFM revealed that the elastic modulus of the brush increased from 1.2 ± 0.1 MPa to 13.7 ± 2.7 MPa when increasing the concentration of Y^{3+} from 0 to 0.5 mM (Figs. 2E, S11, S12). The agreement between SFA and AFM measurements show that multivalent counterions dramatically influence the structure and mechanical properties of the PSS brushes, dictating their *boundary* lubrication properties (Fig. 2E and Fig. S13).

We propose that multivalent ions affect the lubricity of the PSS brushes through two mechanisms: (1) At low concentrations of multivalent salt, multivalency induces three-body electrostatic bridging interactions between PSS chains and (2) at high concentrations of multivalent salt, the brushes undergo a heterogeneous collapse resulting in increased surface roughness. The bridging mechanism mechanism is expected to be stronger for trivalent ions than for divalent ions due to the higher valency. Coarse-grained molecular dynamics (MD) simulations of polyelectrolyte brushes in the SFA geometry were employed to investigate these hypotheses.

MD simulations were performed at two multivalent ion concentrations: "low", where multivalent ions neutralized 10% of the polyelectrolyte brush charge, and "high", where multivalent ions neutralized 100% of the brush charge (*32*). Given the experimental sliding rate of 5 μm/s, ~100 ns of simulation time corresponds to $5x10^{-4}$ nm relative motion of the apposing surfaces, which makes comparison with equilibrium simulations reasonable. Brushes were simulated at a large separation distance where the apposing brushes were relatively non-interacting, and also at high

compression. Trivalent results are presented in Figs. 3, S14 and S15, with divalent results found in Figs. S16 and S17.

Figure 3A,B shows the time-averaged brush density and a representative snapshot of chain conformations at low trivalent ion concentration and large separation, where the brushes exhibited a uniform, extended morphology. When apposing brush layers were brought into close-contact (Figs. 3C, S14), they maintained a uniform extended morphology. When the trivalent ion concentration was increased (Figs. 3D,E,F, S15), the brush layers exhibited lateral phase segregation and collapsed into heterogeneous aggregates; at large separation (Fig. 3D), these aggregates formed independently on each surface, whereas at close-contact (Fig. 3E,F), the apposing brushes formed a unified phase linking the two surfaces. Divalent ions exhibited qualitatively similar results to the trivalent ions, albeit the magnitude of heterogeneous collapse for divalent ions is decreased relative to trivalent ions (Figs. S16, S17). This stronger influence of trivalent ions is corroborated by the simulated brush relaxation dynamics (Fig. S18). Such a scenario is similar to the contact of two rough surfaces with no polyelectrolyte-induced lubrication.

Whereas the structural collapse at high multivalent salt concentration is evidenced by the SFA, AFM, and MD results, the presence of 3-body electrostatic bridging, especially at low concentrations, is not obvious in Fig. 3C,E. To this end, we computed the percentage of multivalent ions bridging apposing polymer brushes as a function of scaled brush separation (ζ) using a topological distance parameter that directly reports whether 3-body bridging correlations occur within the simulations (Fig. 4A). At high and low concentrations, the fraction of trivalent ions bridging the brushes at close contact ($\zeta \sim 0.44$) is ~20%, but these interactions exhibit different

distance dependencies, especially at large separation (Fig. 4A) ($\zeta > 0.55$). At low concentrations, bridging interactions decrease gradually with increased separation, whereas at high concentrations a sharp transition occurs when the brush separation distance cannot support a single spanning collapsed phase. Divalent ions exhibit similar concentration dependencies, but with a smaller overall magnitude of bridging. Simulation results support the hypothesis that electrostatic bridging increases the friction between apposing polyelectrolyte brushes at low multivalent ion concentrations (Fig. 4B,C), and that structural change of the polyelectrolyte brushes dominates the friction at much higher concentrations (Fig. 4D).

Polyelectrolyte brushes have been proposed as efficient boundary lubricants (*2*). This work confirms that the charged polymer chains and the osmotic pressure of the counterions provide excellent lubrication properties in monovalent salt solution. However, the lubrication can break down in the presence of multivalent counterions, even at very low concentrations, resulting from electrostatic bridging between chains from apposing surfaces and changes in surface topology. Our discoveries have implications for developing better water-based boundary lubrication for manmade systems in aqueous or physiological media, such as in biomedical devices.

References and Notes

1 N. B. Holland, Y. X. Qiu, M. Ruegsegger, R. E. Marchant, *Nature* **392**, 799-801 (1998).
2 S. Lee, N. D. Spencer, *Science* **319**, 575-576 (2008).
3 B. Zappone, M. Ruths, G. W. Greene, G. D. Jay, J. N. Israelachvili, *Biophys J* **92**, 1693-1708 (2007).
4 G.E. Fantner *et al.*, *Nat Mater* **4**, 612-616 (2005).
5 T. G. Drummond, M. G. Hill, J. K. Barton, *Nat Biotechnol* **21**, 1192-1199 (2003).
6 E. Karzbrun, A. M. Tayar, V. Noireaux, R. H. Bar-Ziv, *Science* **345**, 829-832 (2014).
7 G. Pardatscher *et al.*, *Nat Nanotechnol* **11**, 1076-1081 (2016).
8 R. Heeb, R. M. Bielecki, S. Lee, N. D. Spencer, *Macromolecules* **42**, 9124-9132 (2009).
9 J. Klein, *Annu Rev Mater Sci* **26**, 581-612 (1996).

10 U. Raviv *et al.*, *Nature* **425**, 163-165 (2003).
11 J. Seror, L. Y. Zhu, R. Goldberg, A. J. Day, J. Klein, *Nat Commun* **6**, 6497 (2015).
12 A. Li *et al.*, *Macromolecules* **44**, 5344-5351 (2011).
13 X. Banquy, J. Burdynska, D. W. Lee, K. Matyjaszewski, J. N. Israelachvili, *J Am Chem Soc* **136**, 6199-6202 (2014).
14 E. B. Zhulina, M. Rubinstein, *Macromolecules* **47**, 5825-5838 (2014).
15 M. Kobayashi, M. Terada, A. Takahara, *Farad Discuss* **156**, 403-412 (2012).
16 O. Al-Jaf, A. Alswieleh, S P. Armes, G. J. Leggett, *Soft Matter* **13**, 2075-2084 (2017).
17 Y. Mei *et al.*, *Phys Rev Lett* **97**, 158301 (2006).
18 S. Sanjuan, P. Perrin, P., N. Pantoustier, Y. Tran, *Langmuir* **23**, 5769-5778 (2007).
19 M. A. C. Stuart *et al.*, *Nat Mater* **9**, 101-113 (2010).
20 J. Yu *et al.*, *Macromolecules* **49**, 5609-5617 (2016).
21 A. Jusufi, O. Borisov, M. Ballauff, *Polymer* **54**, 2028-2035 (2013).
22 J. Yu *et al.*, *Sci Adv* **3**, eaao1497 (2017).
23 N. E. Jackson, B. K. Brettmann, V. Vishwanath, M. Tirrell, J. J. de Pablo, *ACS Macro Lett* **6**, 155-160 (2017).
24 L. Liu, P. Pincus, C. Hyeon, *Macromolecules* **50**, 1579-1588 (2017).
25 B.K. Brettmann, P. Pincus, M. Tirrell, *Macromolecules* **50**, 1225-1235 (2017).
26 R. Farina, N. Laugel, J. Yu, M. Tirrell, *J Phys Chem C* **119**, 14805-14814 (2015).
27 M. Chen, W. H. Briscoe, S. P. Armes, J. Klein, *Science* **323**, 1698-1701 (2009).
28 R. W. Wilson, V. A. Bloomfield, *Biochemistry* **18**, 2192-2196 (1979).
29 D. Bracha, R. H. Bar-Ziv, *J Am Chem Soc* **136**, 4945-4953 (2014).
30 S. Jahn, J. Seror, J. Klein, *Annu Rev Biomed Eng* **18**, 235-258 (2016).
31 M. Ruths, D. Johannsmann, J. Ruhe, W. Knoll, *Macromolecules* **33**, 3860-3870 (2000).
32. Supplementary materials are available on *Science* Online.
33 J. Yu *et al.*, *Polymer* **98**, 448-453 (2016).
34 P. Pincus, *Macromolecules* **24**, 2912–2919 (1991).
35 M. Husseman *et al.*, Macromolecules **32**, 1424–1431 (1999).
36 T., Hoshino, Y. Tanaka, H. Jinnai, A. Takahara, *J Phys Soc Jpn* , **82**, 021014 (2013).
37 N. Maeda, N. H. Chen, M. Tirrell, J. N. Israelachvili, *Science* **297**, 379-382 (2002).
38. P. Mocny, H. A. Klok, Tribology of surface-grafted polymer brushes. *Mol Syst Des Eng* **1**, 141-154 (2016).
39. P. C. Nalam, J. N. Clasohm, A. Mashaghi, N. D. Spencer, Macrotribological Studies of Poly(L-lysine)-graft-Poly(ethylene glycol) in Aqueous Glycerol Mixtures. *Tribol Lett* **37**, 541-552 (2010).

Acknowledgements

We would like to thank Jun Mao and Dean Mastropietro for their assistance with the SFA experiments. **Funding:** JY, JJdP and MT thank the U.S. Department of Energy Office of Science, Program in Basic Energy Sciences, Materials Sciences and Engineering Division. JY thanks a start-up grant of NTU, M4082049.070. NEJ thanks the Argonne National Laboratory Maria Goeppert Mayer Named Fellowship for support. This material is based upon work supported by the National Science Foundation under Grants No. NSF CMMI-1562876 (XX) and NSF CMMI-1161475 (MR). YM and YK were supported by

the Adelis Foundation. We gratefully acknowledge the computing resources provided on Blues, a high-performance computing cluster operated by the Laboratory Computing Resource Center at Argonne National Laboratory. **Author contributions:** JY performed the SFA experiments and data analysis. NEJ performed the molecular dynamics simulations and data analysis. XX, YM, YK and MR performed the AFM experiments and data analysis. JY, JJdP, and MT designed the research. JY, NEJ, YK, MR, JJdP and MT wrote the manuscript. **Competing interests:** The authors declare no competing interests. **Data and materials availability:** all data are available in the manuscript or the supplementary material.

Supplementary Materials
www.sciencemag.org/content/.....
Materials and Methods
Figs S1 to S18
References (32-37)

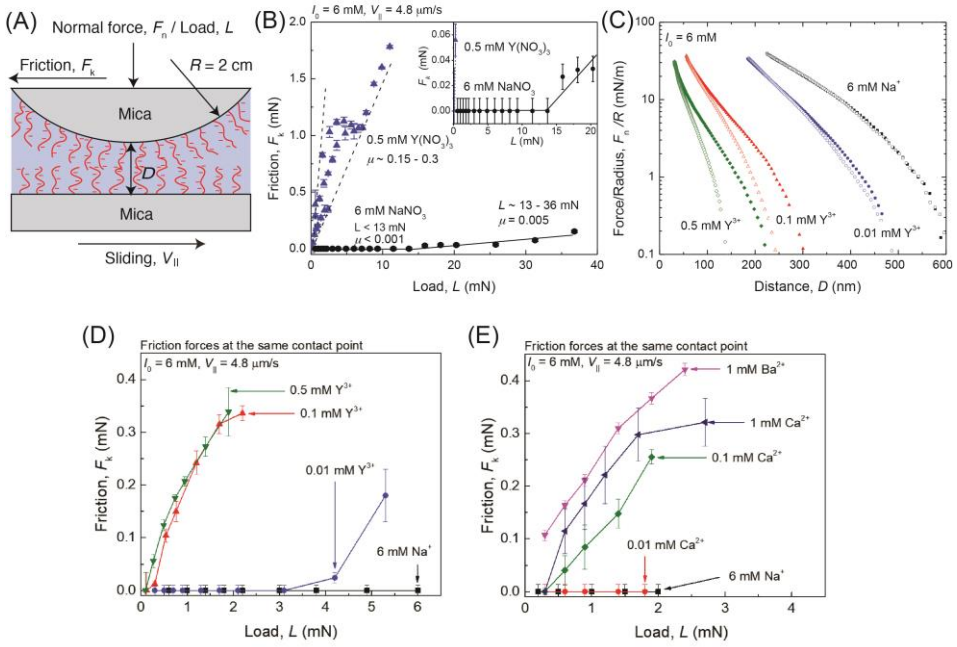

Fig. 1. Forces between apposing PSS brush layers in solution. (A) The geometry of normal force, F_n (also called load, L) and friction force measurements with the SFA. (B) The friction forces between two PSS brush layers in 6 mM $NaNO_3$ (circles), 0.5 mM $Y(NO_3)_3$, and 3 mM $NaNO_3$ (triangles) solutions. (C) Normal force–distance curves and (D) friction forces of apposing PSS brushes measured at constant contact point and ionic strength (6 mM) in 6 mM $NaNO_3$, 0.01 mM, 0.1 mM, and 0.5 mM $Y(NO_3)_3$ and (E) 0.01 mM, 0.1 mM, 1 mM $Ca(NO_3)_2$, and 1 mM $Ba(NO_3)_2$. No damage was detected during the friction measurements. Error bars represent +/- SD, averaged over six to ten repeat measurements.

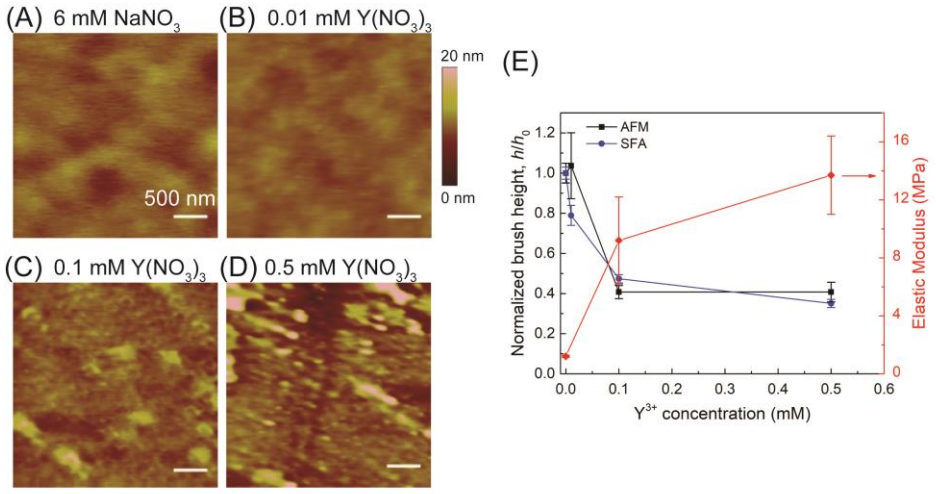

Fig. 2. AFM images and heights of PSS brush layer. (A) 6 mM $NaNO_3$, and (B) 0.01 mM, (C) 0.1 mM, and (D) 0.5 mM $Y(NO_3)_3$ solutions at a constant ionic strength of 6 mM. (E) Normalized brush height, h/h_0, and elastic modulus, E, of the brushes as a function of Y^{3+} concentration. h and h_0 are the heights of the brush in each solution and in 6 mM $NaNO_3$, respectively. Error bars represent +/- SD averaged over the whole AFM image (S11 and S12) for the AFM results and +/- SD averaged over three to four repeat SFA measurements for the SFA results.

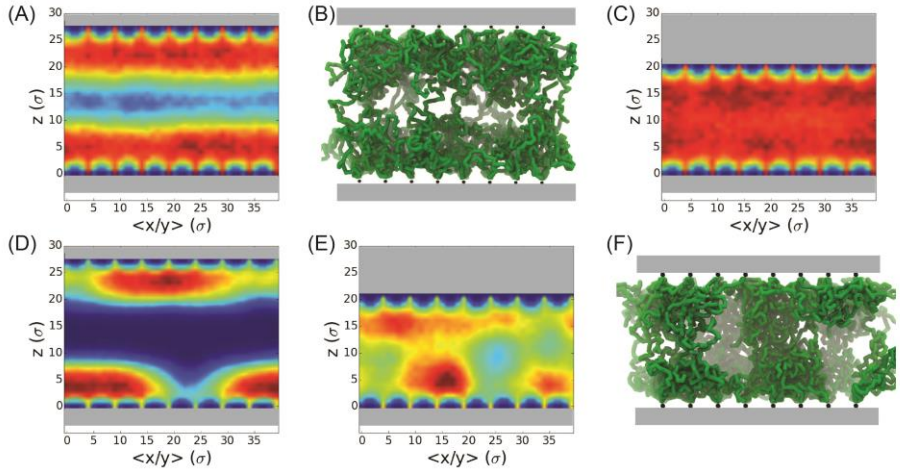

Fig. 3. **MD simulation of apposing polyelectrolyte brushes**. Simulations at low (10% brush charge neutralized by trivalent cations) and high (100% neutralized) trivalent ion concentrations. (A) Brush density at 10% neutralization/29 σ separation and (B) representative MD snapshot showing a uniform, extended morphology at large separation. (C) Brush density at 10% neutralization/22 σ separation showing a uniform extended morphology at small separation. (D) Brush density at 100% neutralization/29 σ separation demonstrating lateral phase segregation at large separation. (E) Brush density at 100% neutralization/22 σ separation and (F) representative MD snapshot showing a unified phase linking the surfaces at close-contact. Heat maps in (A), (C), (D), and (E) correspond to the time-averaged density of polyelectrolyte brush monomers (red = high density) relative to the background (blue = low density). Gray regions represent the mica surfaces. <x/y> denotes an average of the brush density over both the xz and yz planes. Z denotes the vertical separation between apposing brushes, and is proportional to the distance *D* from Fig. 1A. Darker colors in (B) and (F) indicate the foreground, with lighter colors indicating the background.

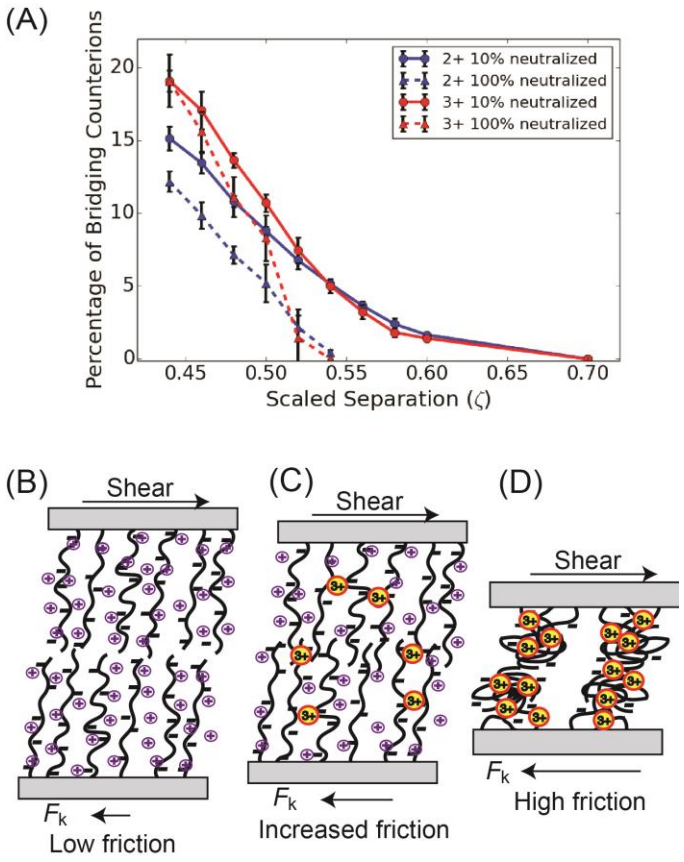

Fig. 4. Multivalent Ion-Induced Friction Mechanisms. MD simulation showing multivalent ion-induced bridging between apposing polyelectrolyte chains at low and high salt concentrations. (A) Percentage of multivalent cations bridging apposing polyelectrolyte chains plotted against the scaled separation distance (ζ), which is normalized by the polymer contour length (50 σ). Error bars represent +/- SD, averaged over five replicas. (B–D) Schematics of apposing PSS brushes sliding against each other in (B) 6 mM $NaNO_3$, (C) 0.01 mM $Y(NO_3)_3$ and (D) 0.1 mM $Y(NO_3)_3$ solution.